Evidence for a Rapid Turnover of Argon in the Lunar Exosphere

Jacob A. Kegerreis[a,*], Vincent R. Eke[a], Richard J. Massey[a], Simon K. Beaumont[b], Rick C. Elphic[c], Luís F. Teodoro[c]

[a] *Institute for Computational Cosmology, Department of Physics, Durham University, South Road, Durham DH1 3LE, U.K.*
[b] *Centre for Sustainable Chemical Processes, Department of Chemistry, Durham University, South Road, Durham DH1 3LE, U.K.*
[c] *NASA Ames Research Center, MS 245-3, Moffett Field, CA 94035, U.S.A.*

arXiv:1612.02414v1 [astro-ph.EP] 7 Dec 2016

Abstract

We have developed a numerical model of the Moon's argon exosphere. The results from our simulations are tested using measurements from the Lunar Atmosphere and Dust Environment Explorer (LADEE) and the Lunar Atmosphere Composition Experiment (LACE). We find that the local time of the near-sunrise peak in exospheric density provides a strong constraint on the nature of the surface interactions of the argon molecules. The time of this peak is the same over both the maria and highlands, and can be reproduced by simple surface interaction models with a single desorption energy of 28 kJ mol^{-1}. The density at all local times of day is also reproduced to within a factor of 2 with the inclusion of a 'squirrelling' process, by which particles build up a subsurface population during the night that reappears the following day. We demonstrate that the persistent enhancement in argon density over the western maria in the LADEE dataset cannot be explained by locally changing the surface interactions over the maria, because this inevitably leads to a decrement at other local times of day, as well as shifting the position of the sunrise peak away from that in the highlands. The only possible explanation for this overdensity appears to be that it is driven by a source coincident with the potassium overabundance in the western maria, and that the average lifetime of argon molecules in the exosphere is very brief (∼1.4 lunar days, 41 days). This implies high source and loss rates of 1.1×10^{22} argon atoms s^{-1}, which could require permanent cold traps comparable with the area of permanently shadowed regions, or a more highly localised source. We demonstrate that the long-term variation in the global argon density seen by LADEE could be explained by the presence of large seasonal cold traps, the required sizes of which depend on the area of the permanent traps.

Keywords: Moon, Atmospheres, dynamics, Moon, surface

1. Introduction

The Moon possesses our nearest example of a surface-bounded exosphere, the most common type of atmosphere in the solar system. As the molecules constituting an exosphere do not interact with one another during their ballistic trajectories over the surface, different species form independent systems. Their exospheric densities and variation with local time depend upon the sources, sinks, and surface interactions for that particular species. Hence, studying the lunar exosphere has the potential to teach us about the solar wind, the lunar interior and outgassing, the efficiency of volatile sequestration in polar cold traps, and the kinetics of adsorption and desorption in low pressure environments (Stern, 1999; Watson et al., 1961; Wieler and Heber, 2003).

Argon is a particularly well-studied species in the lunar exosphere, having been first detected by the Lunar Atmosphere Composition Experiment (LACE), which measured the ^{40}Ar/^{36}Ar ratio at the surface to be approximately 10 (Hoffman et al., 1973). This implied that the more important source of argon was radioactive decay of ^{40}K to ^{40}Ar, rather than solar-wind derived ^{36}Ar. The LACE results showed that the argon exospheric density decreased through the night and had a rapid increase that began just before sunrise, typical

*Corresponding author
Email address: jacob.kegerreis@durham.ac.uk (Jacob A. Kegerreis)

of a condensible gas that adsorbs to the cold nighttime surface and desorbs at dawn (Hodges and Johnson, 1968). In addition to this daily variation, there was a longer term decrease by a factor of approximately 2 seen during the nine lunar days of observations (Hodges, 1975).

The Lunar Atmosphere and Dust Environment Explorer (LADEE) orbital mission produced a wealth of data concerning the lunar exosphere at altitudes from 3–140 km (Elphic et al., 2014). As well as measuring the daily and long-term variations in argon density during its 5 month mission, the Neutral Mass Spectrometer (NMS, Mahaffy et al., 2014) also determined the vertical structure of the exosphere and the variation with selenographic longitude. This led to the discovery that there was an enhancement in the argon exospheric density over the western maria, dubbed the argon 'bulge' by Benna et al. (2015). The long-term variation in the argon abundance was ~28 % during the LADEE mission, much smaller than had been seen 40 years earlier by LACE over similar time periods. However, Hodges and Mahaffy (2016) noted that 'the absence of sensitivity-related tests of the Apollo 17 instrument allows the possibility that the 1973 results were in-part artefacts.'

Different models of aspects of the lunar ^{40}Ar system have been created to help interpret the available data, both in terms of the outgassing rate from the surface and the corresponding sinks that are necessary to yield the measured exospheric density. Hodges (1975) used the LACE data and Monte Carlo methods to simulate an argon exosphere to constrain both the source rate and the surface interactions. Grava et al. (2015) also employed a Monte Carlo technique to follow an initial injection of argon molecules through their lifetimes in the exosphere, concluding that approximately 10 % of the area of permanently shadowed regions (PSRs, Mazarico et al., 2011) needed to cold trap molecules in order to provide a sufficiently high loss rate to match the LACE long-term decline in argon exospheric density. Had a continuous background source been included in their model, larger cold traps would have been required to deplete the exospheric argon density rapidly enough.

Using their model, Grava et al. (2015) suggested that long-term variations in the exospheric density can be ascribed to sporadic moonquakes. Benna et al. (2015) noted the possibility of tidal stress as the source of the LADEE variation. In contrast, Hodges and Mahaffy (2016) proposed that seasonal fluctuations in the total cold trap area are responsible for the smooth, mission-long variations in argon density measured by LADEE (Benna et al., 2015).

More than one proposed explanation also exists for the bulge – the persistent enhancement of exospheric argon localised over the western maria. Benna et al. (2015) noted the similarity between the longitudinal variation in argon and the map of near-surface potassium returned by the Lunar Prospector Gamma Ray Spectrometer (LPGRS, Lawrence et al., 1998). However, Hodges and Mahaffy (2016) asserted that the lifetimes of argon molecules in the lunar exosphere are too long for them to reflect their source locations. Instead, they suggest that the bulge results from lower desorption energies at these longitudes, which would cause argon to spend less time residing on the surface where it cannot be measured.

In this paper, we develop a new model of the lunar argon exosphere using Monte Carlo methods. This approach is similar to those described by Smith et al. (1978), Hodges (1980a), and Butler (1997), in their studies of the helium and water exospheres of the Moon and Mercury. We apply our algorithm to address the questions of what is responsible for the longitudinal and long-term variations in the argon densities measured by LADEE. Specifically, we produce the first simulations with: periodically varying cold trap areas; a source that reflects the lunar near-surface potassium distribution; and spatially-varying surface interactions.

Section 2 contains a description of the data set used and an overview of the different aspects of the lunar argon exosphere that the LADEE data can constrain. Our model is outlined in Section 3, and the results and their implications for the source, sinks and regolith interactions of argon atoms are described in Section 4.

2. Data

The NMS on LADEE measured the density of argon (and other species) in the lunar exosphere from 22nd November 2013 to 17th April 2014 at a wide range of altitudes, longitudes, and local times of day at latitudes within 30° of the equator. Derived data, including background-subtracted argon number densities at altitude, were obtained from The Planetary Atmospheres Node of NASA's Planetary Data System.

We apply two cuts to the entire LADEE argon data set, to produce the subset of data used here. In the full data set, any densities that are negative after the background subtraction (due to noise) have had their values set to zero, which causes the mean to be artificially high if these are either included as zeros or discarded. We only use data in bins of local time of day and selenographical longitude for which more than half of the observations are positive. In this way, the medians of the resulting sets of measurements should not be biased by this prior treatment of negative values. Also, an unaccounted-for temperature dependence of the instrument background can affect the densities just after midnight (M. Benna, personal communication, July, 2016). This problem is only important at this local time of day and for very low densities, where the instrument background was large compared with the signal. We therefore discard data at local times of day $180° - 265°$ (where $0°$ is noon, $90°$ is sunset, $180°$ is midnight, and $270°$ is sunrise). Fortunately, the LACE data largely fill the overnight gap, and we supplement the LADEE measurements using the results presented by Hodges (1975).

Four complementary aspects of the argon exosphere can readily be studied: (1) the change in density with altitude; (2) the long-term variation in the global density during the months of LADEE's operation; (3) the density distribution with local time of day; and (4) the dependence on selenographical longitude, showing the bulge over the western maria (Benna et al., 2015).

2.1. *Densities at Altitude*

In order to study the final three of these distributions, we need to account for the measurement altitude varying from 3 to 140 km. Following convention, and for comparisons with the LACE data, we convert all measurements to the corresponding densities that would have been measured at the surface. To do this, we consider the expression derived by Chamberlain (1963) linking the number density in an exosphere as a function of height, $n(h)$, to the number density and temperature at the surface, n_0 and T respectively. For a spherical body with mass M and radius r,

$$n(h) = n_0 \exp\left[-\frac{GMm}{kT}\left(\frac{1}{r} - \frac{1}{r+h}\right)\right], \qquad (1)$$

where m is the mass of the particle, G is the gravitational constant, and k is the Boltzmann constant. This is the generalised form of the (isothermal) barometric law.

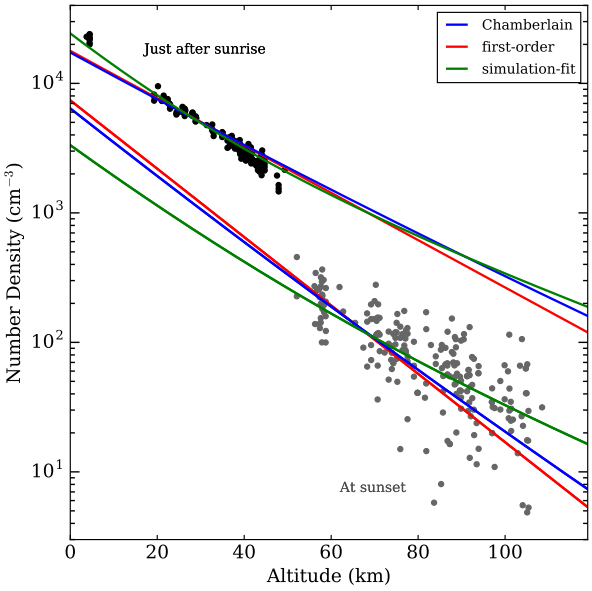

Figure 1: Two examples of the change of density with altitude near the terminators. The black and grey points show the LADEE data just after sunrise (273°) over the maria and at sunset (90°) over the highlands respectively. The coloured lines show the three models at the same local times of day, scaled in magnitude to match the data. The data have had the long-term variation extracted, as described in Section 2.2.

We refer to this as a 'Chamberlain distribution'. The altitude dependence used by Benna et al. (2015), which results from assuming a constant acceleration due to gravity, is the first-order expansion of Eqn. (1) for small h.

The surface temperature varies as a function of latitude and local time, with a particularly rapid variation around the terminators. Lateral transport of molecules implies that the density at altitude will not reflect only the single sub-detector surface temperature, because particles reaching the detector will have originated at a variety of locations and temperatures. Therefore, we expect the real distribution to be a sum of many Chamberlain distributions for different temperatures, weighted by the number of particles that come from each one. As a practical model, we approximate this distribution with a sum of just two Chamberlain distributions at different temperatures and find the best-fit parameters at all times of day using our simulations, as detailed in Appx. A.3.

Fig. 1 shows two illustrative examples of the altitude variation of the LADEE data near to the terminators, where the three models described above differ most

from each other. It is apparent that the choice of extrapolation to zero altitude can significantly effect the inferred number density at the surface.

The LADEE data cover only a small range of altitudes at most local times of day. So, we use our simulations to test how accurately the three different models predict the simulated density at the surface at every time of day, from observations taken at the average LADEE altitude of 60 km. We found that our 'simulation-fit' model of two Chamberlain distributions with different temperatures successfully predicts the density at the surface to within 12 % everywhere. This compares with overestimates as high as 337 % and 416 % for the single Chamberlain distribution and its first-order expansion respectively. These deviations are most pronounced near the terminators. For example, just before sunrise, where the sub-detector surface temperature is very low, many particles will also be detected that originated at the hot surface after sunrise, which the Chamberlain and first-order models cannot account for. Away from the terminators, in regions where the surface temperature varies only slowly with local time of day, all three extrapolations correctly predict the density at the surface to within a few per cent, although the first-order model does less well at higher altitudes. We use the simulation-fit model to infer all LADEE argon densities at the surface reported in this paper.

The agreement of the simulation results with the LADEE altitude data at all local times of day is also good evidence that our underlying models for the simple thermal desorption of argon molecules from the surface are appropriate. This is in contrast to the result found by Halekas et al. (2016), who measured a population of particles at extremely high altitudes that could not have been generated by thermal desorption from lunar surface temperatures. The data also do not show any clear differences between the altitude distributions above the mare and highland regions.

2.2. *Long-Term Variation*

As the argon abundance varies dramatically with the local time of day, to determine the long-term variation we first split the data into bins of 20° in local time. Each inferred density at the surface is normalised by the mean value for that local time of day, and the median long-term deviation away from this mean value is found. These are shown in Fig. 2, along with the weighted mean of all of these curves. The general agreement

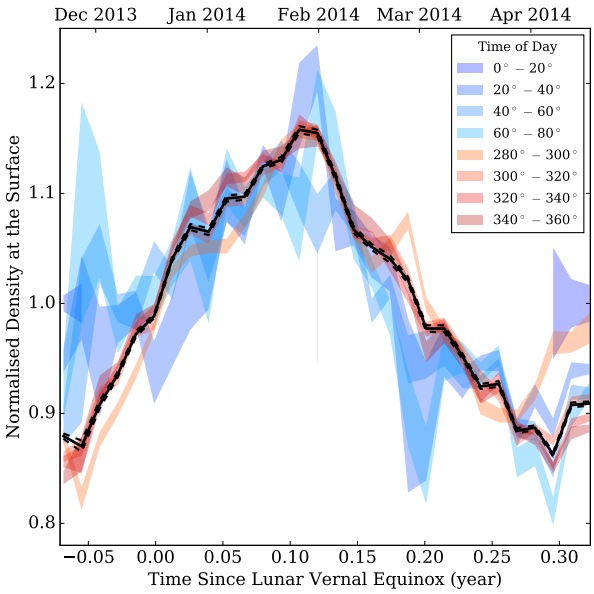

Figure 2: The long-term variation in the LADEE argon density, normalised by the mean density. The different colours show the median variation and its 1σ uncertainty at the corresponding local time of day, as given in the legend. The solid black line shows the total mean variation, weighted by the errors on the time-of-day values. Dashed black lines represent the 1σ uncertainty on this mean. Time is measured from the lunar vernal equinox on 17 December (Archinal et al., 2011).

across the different times of day is notable, as is the relatively smooth variation.

The peak-to-peak change in density is 28 %. Benna et al. (2015) noted the somewhat similar magnitude and timescale of the variation to that observed by LACE, and offered that transient changes in the release rate of argon from the Moon's interior are a plausible cause of this variability. Hodges and Mahaffy (2016) instead suggested that it is part of a periodic fluctuation with a period of half a year. They proposed that this is driven by seasonal variations in the polar cold trap areas.

All subsequent figures in this section show densities at the surface with the mean long-term variation extracted from the data. This is done by dividing each data point by the normalised long-term variation at the time of the measurement. This reveals what LADEE would have observed had the exosphere been in a steady state.

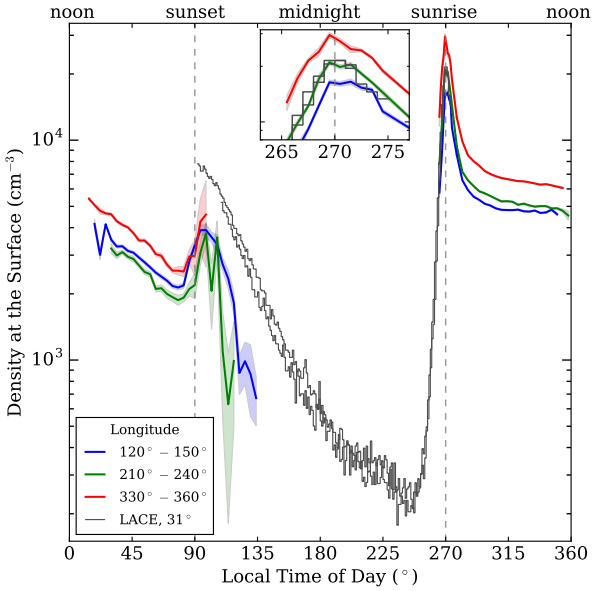

Figure 3: The variation of the argon density with local time of day. The coloured lines are typical examples of the LADEE data across the mare and highland selenographic longitude regions, as given in the legend. The shaded areas represent the $\pm 1\sigma$ uncertainties. The inset plot zooms in on the region around the sunrise peak. The grey lines are two sets of LACE data separated by a few lunar days (Hodges, 1975) and normalised to match the density from LADEE at LACE's location at sunrise. A vertical slice would yield the distribution of density with longitude at that time of day, as shown in Fig. 4.

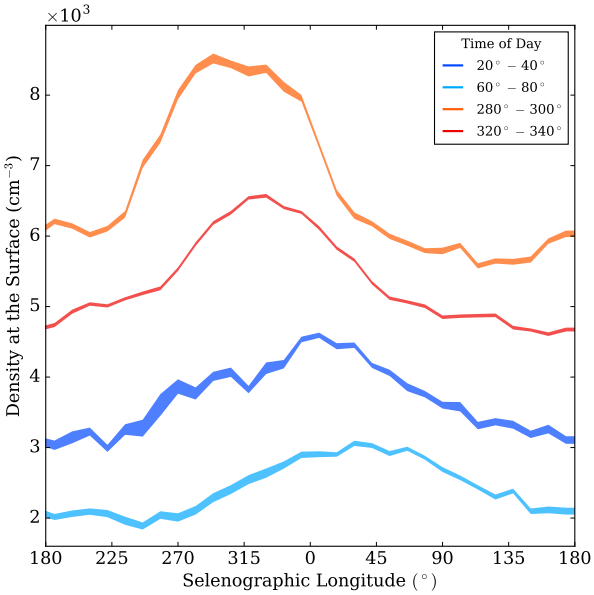

Figure 4: The variation of argon density with selenographic longitude from LADEE, showing the bulge over the western maria and its evolution through the lunar day. The coloured regions show a selection of different local times of day, the shaded areas represent the $\pm 1\sigma$ uncertainties. A vertical slice would yield the distribution of density with time of day at that longitude, as shown in Fig. 3.

2.3. *Local Time of Day*

Fig. 3 shows the distribution of argon with local time of day from LADEE and LACE data, with the LADEE data corrected for altitude and long-term variability as described above. The figure shows just three representative examples across the mare and highland regions for clarity. The LADEE (and LACE) data show very similar behaviour at all selenographic longitudes. In particular, the timing of the sunrise peak is insensitive to the longitude, as highlighted by the inset panel, occurring at local times between 269° ± 1° and 272° ± 1°. However, the argon density is greater in the maria than that in the highlands by a factor that ranges from a few tens of per cent up to almost a factor of 2 at sunrise. The LACE densities have been rescaled in amplitude to match the inferred surface density at sunrise from LADEE at the location of LACE, to extract the long-term variation between the datasets.

The large peaks in density around sunset and sunrise are both fed by particles migrating away from noon, where the higher temperatures mean larger hops. At sunset, the temperature is lower, so particles do not hop very far, but it is not yet cold enough to trap argon on the surface for long periods of time. Any particles that do stick to the surface at night will rotate with the Moon towards sunrise, creating the enormous peak when they warm up at dawn and re-enter the exosphere. This peak extends back into the night because the particles fly in all directions, with a typical hop distance of a few degrees at post-sunrise temperatures.

2.4. *Selenographic Longitude – the Bulge*

The change of density with selenographic longitude is shown in Fig. 4 for different slices in local time of day. As was evident from Fig. 3, the density at all local times of day is highest at some point over the maria (longitudes from 270° – 45°) The peak near sunrise is located over the western maria in the region of the Procellarum KREEP Terrain (PKT), which is rich in ^{40}Ar's parent, ^{40}K (Jolliff et al., 2000). Along the different curves of fixed local time, the selenographic

longitude of the peak argon density drifts systematically from ~300° at sunrise to ~45° at sunset.

These distributions all reflect a complex interplay between sources, sinks and, most importantly, surface interactions of the argon atoms. Consequently, the variation of argon density with both selenographic longitude and local time of day offer the opportunity to distinguish between different models for the argon exosphere.

3. Model

In this section, we describe the main processes and input parameters in our model. Appx. A contains full details of aspects of our model that differ from similar previous studies such as that by Butler (1997). The simulation code itself is released to the public and is available with documentation at icc.dur.ac.uk/index.php?content=Research/Topics/O13.

The central idea is to follow one particle at a time throughout its life, then repeat this for many particles to build up a model of the lunar argon exosphere. Each simulation particle represents a packet of argon flux, and in between its creation and eventual loss from the system, it migrates in a series of interactions with the surface and ballistic hops. The models for each of these various processes are now described in turn.

3.1. Source

Most of our simulations are for a steady-state exosphere in which the continuous source rate matches the loss rate, after an initialisation period in which more particles are created than are lost. The source rate, the mean lifetime, and the total number of particles in the equilibrium system are directly related – knowing any two determines the third. In our simulations, we choose the mean lifetime of the particles by varying the sinks, and the total amount of argon in the exosphere is then scaled to match that from the LADEE measurements by fixing the source rate.

The value for the source rate is implicitly varied in a range that reflects the uncertainty in the amount of potassium in the Moon and the effectiveness with which radiogenic ^{40}Ar reaches the surface. Killen (2002) modelled argon's production and diffusion from the potassium in the crust and estimated that argon enters the exosphere at a rate in the range of $3.8 - 5.5 \times 10^{20}$ atoms s^{-1}. These values correspond to only a few per cent of the ^{40}Ar that is created inside the Moon (Hodges, 1975), so we also investigate significantly higher source rates.

We wish to test if a local source can reproduce the argon bulge over the western maria and, if so, what this would require. Thus, we use either a global source, where the argon particles appear isotropically at random locations on the spherical surface, or a local source, where they appear preferentially at locations with higher near-surface potassium concentrations. The LPGRS, and more recently gamma-ray spectrometers on board Chang'E-1 and Chang'E-2, measured the potassium abundance and distribution in the top metre or so of the regolith (Prettyman et al., 2006; Zhu et al., 2011, 2015). We use the LPGRS potassium map to weight the source distribution for the simulation particles such that the probability of being sourced at a given location is proportional to the local potassium concentration.

3.2. Sinks

There are two main ways in which particles can be lost from our simulations: interactions with photons or charged particles from the sun; and cold trapping on the surface in the permanently shadowed polar regions. Our implementation of these physical processes is described in the following subsections. We include the possibility of gravitational escape in our simulations, but for argon this has a negligible effect.

3.2.1. Solar Radiation

A particle in flight on the dayside may be lost due to a variety of processes, the most important of which are photoionisation and charge-exchange with solar wind protons (Grava et al., 2015). An ionised particle will rapidly be driven either away from or into the Moon's surface by the local electromagnetic field. Those that impact the surface may be neutralised and 'recycled' back into the exosphere. Following Butler (1997), such processes can be combined to give a single solar radiation destruction timescale, $\tau = 3.14 \times 10^6$ s (Grava et al., 2015). This includes an assumed recycling fraction of 0.5 (Poppe et al., 2013) simply by doubling the timescale, which is analogous to assuming that a

recycled ion re-enters the exosphere without travelling for a significant time or distance. The probability of loss during a flight of time t is then

$$P(t) = 1 - e^{-t/\tau} \ . \tag{2}$$

For each particle hop, our algorithm picks a random number from a uniform distribution between 0 and 1. If this lies below $P(t)$, then the particle is removed from the simulation.

3.2.2. *Cold Traps*

If a particle lands in a permanent cold trap near the poles, then it is assumed to stick there indefinitely. Like previous models, we adopt a stochastic approach. When a particle lands within 15° of the north or south pole, it has a probability of being trapped, given by the total fractional area of cold traps in that polar region. Various estimates have been made for the size and distribution of cold traps. The appropriate cold trap area depends on the surface interaction of the specific species and the complicated processes that may occur after landing in a cold trap, either to secure or remove the particles (Schorghofer and Taylor, 2007; Chaufray et al., 2009). As the uncertainty on the effective cold trap area is large, we leave this as a free parameter.

Fig. 5 shows the mean lifetime (and corresponding source rate) for different cold trap areas, keeping the photodestruction timescale constant and using the surface interaction models described in the following subsection. Larger cold traps result in shorter lifetimes, and a larger source rate is then required to maintain the same total number of argon atoms. Also shown in Fig. 5 are the maximum surface temperatures that correspond to certain cold trap areas, as inferred from Diviner data (Vasavada et al., 2012). This is done by relating a given cold trap area to the same-size area that never exceeds a certain temperature.

For our default surface interaction model, the total argon content in the simulation is set at 4×10^{28} atoms to match the LADEE abundance measurements. The main uncertainty in this number arises from the long-term and selenographic variations in density measured by LADEE, amounting to about 44 %.

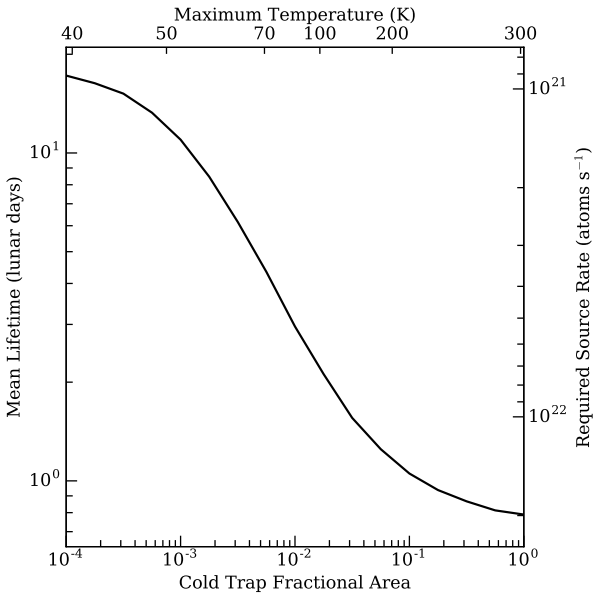

Figure 5: The mean lifetime of the simulated argon particles for different cold trap areas as fractions of the polar 15°. The right axis shows the source rate of argon that would be required to match the inferred LADEE total argon abundance. The top axis gives the maximum surface temperatures from Diviner that correspond to the assumed areas covered by cold traps.

3.2.3. *Seasonal Cold Traps*

We include the possibility of seasonal cold traps in our model in addition to the permanent cold traps. These have fractional areas in the north and south polar 15° that grow and shrink periodically as

$$\begin{aligned} f_{\rm N} &= \max\left[0,\ f_{\rm peak}\sin\left(2\pi\,(t_{\rm yr} - 0.5)\right)\right] \\ f_{\rm S} &= \max\left[0,\ f_{\rm peak}\sin\left(2\pi\,t_{\rm yr}\right)\right] \ , \end{aligned} \tag{3}$$

where $f_{\rm peak}$ is the peak fractional area and $t_{\rm yr}$ is the time in units of years. Thus, the year begins with the vernal equinox and the southern trap reaches its maximum size one quarter of the way through the year, followed by the autumnal equinox and the northern peak in turn. A particle that lands in a seasonal cold trap is released back into the exosphere at a random subsequent time when the seasonal cold traps at the relevant pole have shrunk appropriately, accounting for the distribution of the times at which the traps first appeared (and hence the times at which they will disappear).

3.3. Hop Trajectory

In the absence of forces other than the gravity from the Moon, the complete paths of particles – including the landing position, time of flight, and position and velocity at any altitude – can be calculated analytically from the starting location and velocity using Kepler's laws (see Appx. A.2). This approach is much less computationally intensive than integrating the paths numerically, even when positions and velocities are also calculated at altitude. This is how we transport particles in our simulation and, apart from the time of flight, it matches the approach of Butler (1997) and Crider and Vondrak (2000) for finding the landing position. For their time of flight calculation, they effectively assumed that the surface is flat, leading to slightly underestimated flight times.

For the initial velocity, the particles are assumed to have accommodated to the surface temperature at their starting location and to have a Maxwell-Boltzmann distribution in the exosphere for that temperature. This means that the initial speed for a particle leaving the surface must be drawn from the Maxwell-Boltzmann flux distribution (Brinkmann, 1970; Smith et al., 1978). As each particle represents a small packet of argon flux moving through the surface, the random emission direction in the outwards hemisphere needs to be weighted by the component of the speed in the vertical direction. The good fit of the simulation densities at altitude to the LADEE data suggests that this model is appropriate. Another difference between our treatment and those of Butler (1997) and Crider and Vondrak (2000) is that they chose emission angles away from vertical, α, from a non-isotropic distribution that was uniform between 0 and $\pi/2$, without including the $\sin(\alpha)$ term that accounts for the full area of the emission hemisphere.

3.4. Surface Interaction

The interaction of argon with the surface determines many of the exosphere's characteristics. However, it is a complicated and poorly-understood process. In our model, once a particle lands it is assumed to adsorb immediately. During the lunar night, the simulated particle may also 'squirrel' down into the regolith, to resurface at some time the following day. Otherwise, or after re-emerging, the particle will reside upon the surface for some amount of time before being desorbed. The residence time and the kinematics of the desorbed particle both depend sensitively upon the temperature at the location of the particle.

The Diviner radiometer on the Lunar Reconnaissance Orbiter (LRO) produced temperature maps of the lunar surface (Vasavada et al., 2012). We use the analytical fit to the Diviner data from Hurley et al. (2015) to make a map of temperature as a function of local time and location in square-degree bins. Following Hurley et al. (2015), we also introduce a longitudinal Gaussian scatter with $\sigma = 4.5°$ into this map to account, statistically, for topographical relief.

3.4.1. Residence Time and Desorption

Every $\Delta t = 5$ s (a time step is only introduced in this part of the simulation), the temperature is re-calculated for particles residing on the surface. This allows a residence time, $t_{\rm res}$, to be found using a standard modified Arrhenius equation (Bernatowicz and Podosek, 1991):

$$t_{\rm res} = \frac{h}{kT} \exp\left[\frac{Q}{RT}\right] , \tag{4}$$

where h is Planck's constant, R is the gas constant, T is the temperature, and Q is the desorption energy.

The probability of the particle desorbing from the surface in a given time step is

$$P(t_{\rm res}) = e^{-\Delta t / t_{\rm res}} . \tag{5}$$

If a uniform random number between 0 and 1 exceeds P, then the particle is released and hops again. Otherwise, the simulation time is advanced by Δt and the particle's position and the local temperature are updated. This continues until the particle is released.

For argon, a barrier-free adsorption process is expected, so heats of adsorption and activation energies for desorption can be equated, both corresponding to Q. Experiments with argon on non-lunar aluminosilicates and mineral oxides have shown that the desorption energy is typically around 8–10 kJ mol^{-1} (Matsuhashi et al., 2001). This increases slightly for more Lewis acidic materials, although higher values were obtained for the heat of adsorption, up to 24 kJ mol^{-1} for some acidified mineral oxides, possibly being representative of lower coverages or corresponding to a small fraction of more strongly adsorbing sites. The surface composition of the moon is dominated by anorthosite,

comprised primarily of a variety of silicate minerals (Cheek et al., 2013; Wieczorek et al., 2006). Therefore, these terrestrial experiments provide a reasonable basis for estimating plausible values of Q.

On a low-energy metal oxide surface facet, Dohnálek et al. (2002) calculated the coverage-dependent desorption energy for argon from temperature-programmed desorption (TPD) data and found it to increase from 8 kJ mol^{-1} to around 13 kJ mol^{-1} at very low coverages (where only the highest energy sites should be occupied). If surface diffusion occurs readily and the coverage is low, then these strong adsorption sites may be accessible to all adsorbing argon atoms. Direct calorimetric heats of adsorption on another porous silica yielded Q values of 18 kJ mol^{-1} (again at low surface coverages of argon, Dunne et al., 1996). Interactions with the pristine lunar regolith may be even stronger (Farrell et al., 2015), and Bernatowicz and Podosek (1991) found with a freshly-crushed lunar sample that somewhat-higher energies of up to 31 kJ mol^{-1} (7.4 kcal mol^{-1}) are plausible.

3.4.2. *Squirrelling*

Argon particles enter the exosphere by migrating up through the porous regolith from the Moon's interior (Killen, 2002). We propose that some proportion of the particles residing on the surface will migrate randomly downwards as well, to re-enter the exosphere at a later time. A somewhat similar process has been discussed in Hodges (1982) and modelled for water ice in polar cold traps by Schorghofer and Taylor (2007).

The persistent reservoir of adsorbed particles residing on the surface at night would therefore act as a source for building up a distribution of particles with depth by the end of the night, which then re-emerge during the day. Appx. A.4 shows that these timescales arise naturally from the regolith structure and temperature. We assume that particles on the dayside do not adsorb frequently enough for long enough to 'squirrel' in significant numbers.

We use a very simple model to investigate the effect this process has on the exosphere. Any particle residing on the nighttime surface is given a small probability, P_{sq}, of becoming buried in the regolith. If this happens, then the particle will re-enter the exosphere at some point during the following day, with a uniform probability distribution.

It is likely that this process is much more complicated in reality, with a dependence on temperature, gradients of temperature and density, and other factors. As one such example, just after sunrise, the subsurface is colder than the surface. This temperature gradient would discourage particles from migrating upwards, perhaps delaying the resurfacing of some squirrelled particles until later in the day than would otherwise be expected. Given these uncertain issues, we note the necessary simplicity of this model, and use it to explore the plausible effects of the process.

The uncertain surface interaction parameters Q and P_{sq} are varied in the next section, to determine the best values to describe the LADEE and LACE results.

4. Results and Discussion

In this section, we compare our simulations with the data introduced in Section 2. First we show how the treatment of surface interactions affects the variation of argon with local time of day. Then we investigate the competing hypotheses to explain the argon bulge over the western maria. In the final part of this section, we study the possibility of seasonal cold traps being the cause of the long-term variation in the LADEE argon abundance.

4.1. *Distribution with Local Time of Day*

The sensitivity of the simulated exosphere to the values of the model parameters describing the surface interactions is shown in Fig. 6. In the left panel, the desorption energy, Q, is varied by ~20 % with the squirrelling process switched off, whereas the right panel shows how the distribution changes when the squirrelling probability, P_{sq}, is altered with fixed $Q = 28$ kJ mol^{-1}.

While the higher desorption energy curves best match the nighttime rate of decrease of argon observed by both LACE and LADEE, these model surfaces are so sticky that the timing of the sunrise peak is delayed too far into the day to match the measurements, as highlighted by the inset panel. The sunrise peak position is sensitively dependent upon the model desorption energy. Given

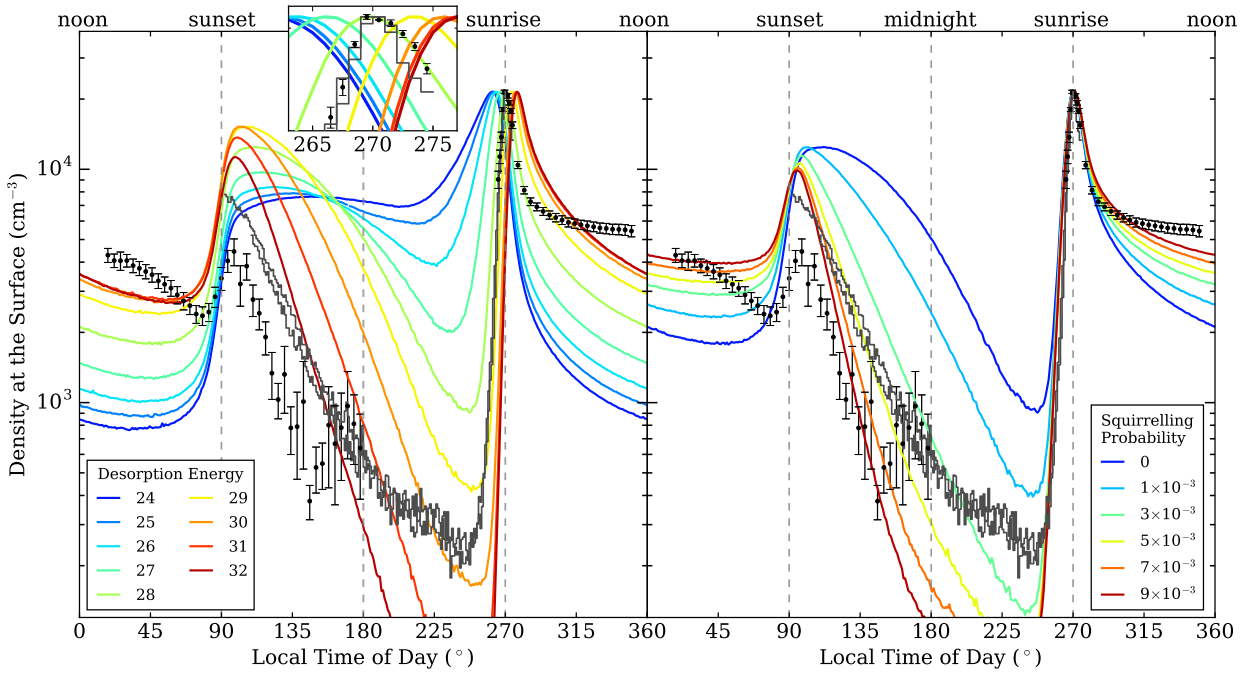

Figure 6: The variation of the argon density as a function of local time of day. For the left panel, the desorption energy is varied and no squirrelling is included. The labels show the model desorption energy, Q, in kJ mol^{-1} and the inset plot zooms in on the region around the sunrise peak. For the right panel, Q = 28 kJ mol^{-1} and the model squirrelling probability is varied as shown in the legend. In both panels, the distributions are normalised to match the peak data density to aid comparison of the shape. The mean data from LADEE across all longitudes are shown with black points and the LACE data are shown with grey lines.

that the sunrise peaks are at the same local time over the highlands and maria (Section 2.3), this suggests that the argon interactions with the surface are similar in these different regions.

Fixing the desorption energy at Q = 28 kJ mol^{-1}, in order to match the sunrise peak position, the model predicts too much exospheric argon late in the night and too little during the day. This provides empirical motivation for the inclusion of our squirrelling process, which allows argon atoms to build up a subsurface population in the regolith overnight that is released during the following day. Increasing P_{sq} enables us to produce a model that matches the nighttime decrease in argon and the shape of the sunrise peak, as shown in the right panel of Fig. 6. For our fiducial value of $P_{sq} = 5 \times 10^{-3}$, the simulation agrees within a factor of 2 with the observations over the entire lunar day. The behaviour from mid-morning to sunset is somewhat discrepant, but given the simplicity of our model and the fact that these details do not change any of the subsequent results and conclusions, we choose not to complicate the model further.

In contrast to our squirrelling approach, Hodges and Mahaffy (2016) adopted a bespoke temperature-dependent desorption energy (up to ~120 kJ mol^{-1} at noon) to bring their model into agreement with the LADEE measurements. Introducing all of this freedom into the model can lead to a good fit, but, as Hodges and Mahaffy (2016) themselves noted, such high desorption energies do 'not comport with thermal energies'. The energies required by their model during the day are far beyond the bond strengths that argon has been measured to make or could be expected to make for the simple van der Waals interactions of a noble gas, as discussed in Section 3.4. Any variable-energy model cannot affect the dayside densities significantly without resorting to such high values, because the high dayside temperatures make the residence times for any lower desorption energies negligible. Note that we also tested a similar model for use in the following bulge and long-term investigations, and the subsequent conclusions were unchanged.

While our squirrelling approach provides a mechanism for fitting the nighttime and daytime argon abundances

using physically plausible desorption energies, the simplifications that this model entails should be noted. These processes have not been extensively studied with argon on terrestrial materials, let alone in situ (Dohnálek et al., 2002). In reality, there will be a range of adsorption sites with somewhat-different desorption energies, and the probability of adsorption will vary depending upon both the speed of the incoming atom and the presence of volatiles already on the surface. For instance, experiments show that argon has about a 70 % probability of adsorbing to a surface at typical exospheric impact speeds of 300 ms^{-1} but much lower temperatures of 22 K (Dohnálek et al., 2002). This probability decreases rapidly with higher impact speeds, reaching zero for 550 ms^{-1}. Argon is also more likely to stick when other argon atoms are already residing on the surface (Head-Gordon et al., 1991). The 300 ms^{-1} adsorption probability reaches one when the coverage is roughly a monolayer. These values may of course be somewhat different for adsorption to the lunar regolith.

We ran additional simulations to investigate the sensitivity of our results to these adsorption issues. Lowering the adsorption probability has a similar effect to lowering the desorption energy. Even for an adsorption probability below 0.1, an increase of a few kJ mol^{-1} to Q results in a similar distribution and sunrise peak position. A speed-dependent adsorption probability also does not dramatically change the distribution, compared with the effects from changing Q or P_{sq}. More importantly, no such mechanisms appear to reduce the need for the squirrelling process to match the high dayside densities. So, while these known simplifications affect the results at a level that could explain some of the small discrepancies between the model and data distributions, our main conclusions are not sensitive to these assumptions.

One final consideration is the cold trap area and corresponding source rate. The above simulations were all run with the low permanent cold trap fractional area of 0.01 % that approximately corresponds to the low source rates estimated by Killen (2002). The much larger traps and high rates considered in the next section have the effect of increasing the density towards the end of the night, which improves the match to the minimum LACE densities (although these may be below LACE's sensitivity (Hoffman et al., 1973)), due to the emergence of newly created particles through in the night. The distribution is unaffected at other local times of day.

4.2. *Longitudinal Bulge*

There are two alternative hypotheses for the origin of the argon bulge over the western maria: (1) it reflects a spatially-variable source rate that is higher over the potassium-rich western maria (Benna et al., 2015); or (2) it reflects a lower desorption energy from the western maria (Hodges and Mahaffy, 2016). We perform simulations using either a local source reflecting the LPGRS potassium map or a uniform global source and a spatially-varying desorption energy to examine these two scenarios.

For the case of a local source with a greater release of argon over the potassium-rich western maria, the amplitude of the bulge depends sensitively upon the source rate, or – equivalently in the steady-state – the loss rate. A rapid turnover of particles with short lifetimes is necessary to produce argon atoms that have not travelled so many times around the Moon that their locations no longer reflect their origin. We ran simulations with a local source (proportional to the LPGRS potassium abundance) with a range of cold trap fractional areas to determine the area required to produce a bulge comparable with that observed by LADEE.

Fig. 7 shows the amplitude of the post-sunrise (280° – 300°) argon bulge over the western maria. As shown by the dashed lines, to match the LADEE maximum-to-minimum ratio of 1.5 ± 0.1, a cold trap fractional area of 4 ± 1 % of each polar 15° is necessary, corresponding to a mean lifetime of ~1.4 lunar days. This area is comparable with the 2 – 2.5 % covered by PSRs (Mazarico et al., 2011), but is uncomfortably large if argon is only supposed to be permanently trapped in regions with temperatures never exceeding ~40 K (Hodges, 1980b). As indicated in Fig. 5, cold traps of this large size appear to correspond to regions with temperatures that can reach up to 175 K.

Therefore, for this to be a viable model, one would need argon to be more readily lost from the exospheric system than previously anticipated, or to have a more highly localised source below the surface than the LPGRS near-surface map. For the extreme case of a top-hat source in the mare region, the same amplitude bulge is produced by a cold trap fractional area of only 0.4 % and a lifetime of 5.3 lunar days. Feasible causes of increased losses could be: an abundance of small-scale cold traps such as those inferred on Mercury (Paige et al., 2014); the presence of other volatile

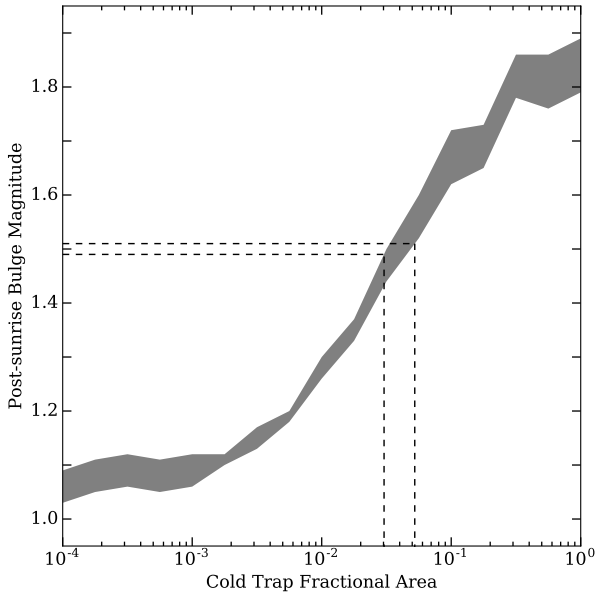

Figure 7: The magnitude of the simulated bulge over the western maria (at 280° – 300° local time of day), generated by the local source, for different values of the cold trap fractional area of the polar 15°. The dashed lines show the magnitude and uncertainty of the bulge measured by LADEE at the same local time, and the corresponding range of cold trap areas.

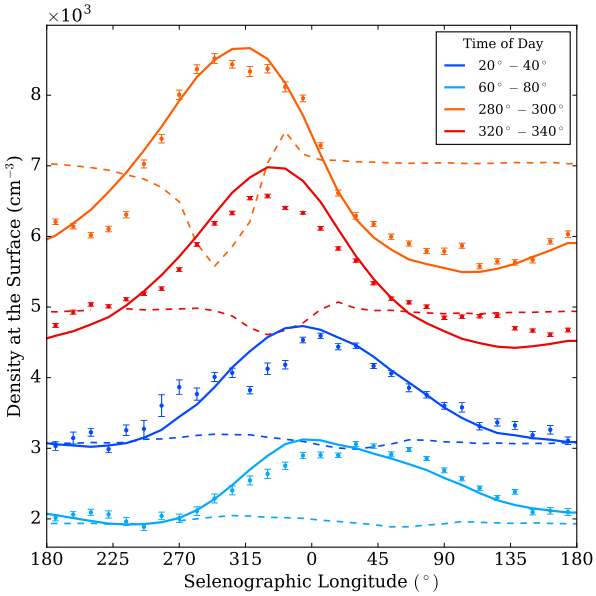

Figure 8: The variation of argon density with selenographic longitude for a representative selection of local times of day, shown by the different colours as defined in the legend. The solid lines show the bulge from the local source model with high rates of source and loss, the LADEE data are shown as points, and the dashed lines show the results for the global source with a lower desorption energy in the mare region than in the highlands (26 and 28 kJ mol^{-1} respectively).

molecules in PSRs increasing the adsorption probability (Dohnálek et al., 2002); and an extra loss mechanism that means that our assumed solar radiation loss rate is an underestimate. Noting this tension, we press on to investigate the shape of the argon bulge in the simulation with a cold trap fractional polar area of 4 % and compare it with the data.

The variation of argon density with longitude in our simulations is shown in Fig. 8 for a sample of different local times of day, with the solid lines resulting from a local source, and the dashed lines from the alternative hypothesis of an isotropic source with mare and highland desorption energies of $Q = 26$ kJ mol^{-1} and 28 kJ mol^{-1} respectively. Also reproduced are the LADEE results. We are predominantly interested in the shapes of the different curves, and not their relative amplitudes, which are determined by the local time of day distribution and are slightly different at certain times, as discussed in the previous section. Thus, for clarity, each model curve was divided by its mean and multiplied by the mean of the corresponding data set.

The model with the local source was tuned only to match the maximum-to-minimum ratio of the post-sunrise argon bulge over the western maria observed by LADEE. However, the relative sizes of the bulge at all other times of day, the position, width, and shape of the bulge, and the shift of the bulge to the east throughout the day also happen to be reproduced well. These features result from the fact that the overnight build-up of argon over the western maria around longitudes ~300° – 330° diffuses rapidly across the sunlit surface after it reaches sunrise. This diffusion spreads out the peak in the argon density and shifts it into the dayside: that is, to the east.

In contrast to the successes of this local source model, the effect of decreasing the adsorption energy over the western maria, shown by the dashed lines in Fig. 8, does not match any of the features in the data. The failure to reproduce the observations arises because the lower desorption energy encourages atoms to leave the surface and hop more frequently. This is successful in producing a bulge towards the end of the night, where the residence time is longest. However, it also rapidly evacuates the argon from the maria, and the nighttime bulge is replaced by a deficit in argon density almost

immediately after sunrise. Therefore, trying to create a local overdensity in this way will inevitably fail if the bulge is required to persist throughout the day, as it is observed to do.

A separate reason to doubt this explanation is that these small changes in adsorption energy lead to significantly different local times for the sunrise peak in the mare and highland regions, in contrast to what the LADEE data show. Consequently, a spatially-varying desorption energy explanation for the argon bulge can be ruled out for a couple of reasons. Similar arguments can be used to dismiss the idea that the bulge results from hotter surface temperatures for the maria, for example.

The local source is the only hypothesis that has the potential to reproduce the variation of argon density with selenographic longitude seen in the data, and the results are remarkably similar. For this explanation to be successful, the lifetime of an argon molecule in the exospheric system (i.e. from source to sink) needs to be ~1.4 lunar days, assuming that the source rate is proportional to the LPGRS potassium abundance. Given the uncertainties in the process of outgassing, the required source rate of 1.1×10^{22} atoms s^{-1} is not immediately implausible. However, the loss rate that this implies appears to demand widespread polar cold-trapping of argon that exceeds what had previously been considered. Assuming that the cold traps have been stable for ~1 Gyr (Arnold, 1979), this means that the order of 10^{13} kg of argon has been delivered to the polar regions during this time.

With this empirical high cold trap fractional area of 4 %, we found that it takes roughly 6 lunar days from the start of the simulation before the exosphere reaches an equilibrium of source and loss rates and a stable number of argon atoms. In comparison, the time it takes for the equilibrium shape of the distributions to become established is always very short, on the order of 1 lunar day. This timescale is the same even with much smaller cold traps, for which the system can take a long time to reach a true steady state. This is analogous to saying that a localised event diffuses rapidly across the system, even if the total number of particles is still offset from equilibrium.

In the steady state: 90 % of particles are lost to cold-trapping and 10 % are removed by solar radiation; the mean particle lifetime is 1.4 lunar days, of which on average 60 % is spent residing on the surface, 30 % squirrelling under the surface, and only 10 % in flight in the exosphere. The total number of argon atoms in the simulated exosphere at any time is about 4×10^{28}, corresponding to a mass of 2600 kg.

4.3. Long-Term Variation

Hodges and Mahaffy (2016) proposed that seasonally-varying cold traps could produce a periodic signal responsible for the smooth long-term variation in the argon exospheric density by 28 % over the 5 months of LADEE's operation. As described in Section 3.2.3, we have included seasonal cold traps to account for the fact that, due to the 1.54° declination of the Moon, when one pole is tilted away from the sun, larger areas will act as cold traps for a few months. These seasonal traps would both temporarily remove and add argon, so they could drive changes in the density on the relevant timescale without a change in the overall source and loss rates.

The magnitude of this variation is affected by the peak size of the seasonal traps and also by the source and loss rates, which in our model are controlled by the sizes of the permanent cold traps. For the low permanent cold trap fractional area of 0.01 % that corresponds approximately to the low source rate estimated by Killen (2002) (where solar wind losses dominate), the 28 % change in the density seen by LADEE was reproduced with a peak seasonal cold trap fractional area of $f_{\mathrm{peak}} = 0.8$ % at each poles' midwinter.

The periodic long-term variation that is produced by these seasonal traps, at the latitudes probed by LADEE, is shown by the solid lines in Fig. 9, over a period of 1 year in the simulation. The peak density is predicted to be delayed by about 0.07 years (1 lunar day, ~1 month) after the minimum trap size at the equinox. This is related to the time it takes for argon to travel between the poles and the equator, and is remarkably similar to the delay in the LADEE data after the lunar vernal equinox, as shown in Fig. 9. Also shown is how much argon becomes trapped and released at each point in time throughout the year by the seasonal traps. Particles can be trapped from the beginning of winter until the very end, but are only released starting after midwinter, when the traps begin to shrink. This leads to a mild asymmetry in the long-term variation, which could easily be modified by deviating from our simple sinusoidal model.

For the larger permanent trap areas (4 %) and higher

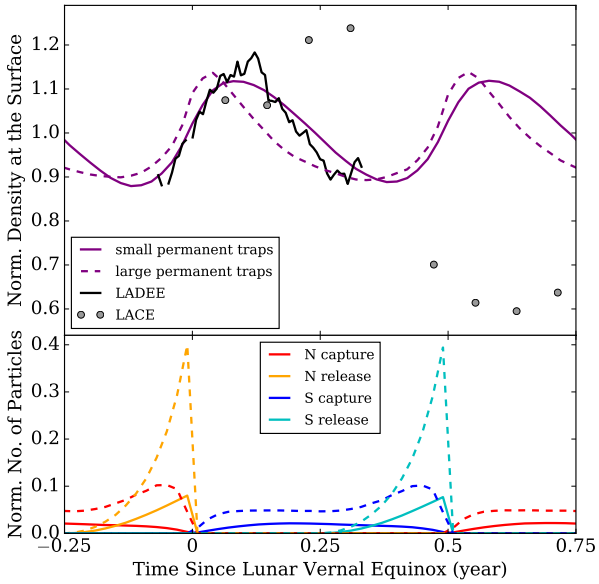

Figure 9: Upper panel: The long-term variation of the argon population within 30° latitude of the equator, normalised by the mean density. The purple solid line shows the normalised simulated density at the surface for the low rates model with permanent and peak seasonal cold trap fractional areas of 0.01 % and 0.8 % respectively; and the dashed line for a high rates simulation with the bulge-generating areas of 4 % and 16 %. Time is measured from the last lunar vernal equinox. The LADEE data is shown by the black line for comparison, and the grey points show the relative magnitudes of the LACE sunrise peaks. Lower panel: The number of argon particles that are being captured and released in each simulation by the northern and southern seasonal traps, given as a fraction of the total number of argon atoms in the equilibrium system (4×10^{28}).

rates that produce a bulge similar to the LADEE data, much larger seasonal traps are needed to cause the same magnitude variation, with a peak fractional area of 16 %. This is because, with much shorter particle lifetimes, fewer particles near the equator have been affected by the seasonal traps. In this case, a maximum of about 2.6×10^{28} argon atoms (over half of the steady-state exosphere) must be temporarily trapped to effect the 28 % variation near the equator, over twice as much as in the low loss case. As shown by the dashed line in Fig. 9's top panel, the delay of the peak density is also affected and occurs 0.04 years (0.5 lunar days) earlier. This timescale is sensitive to the evolution of the seasonal traps. It is possible that unaccounted-for factors such as thermal inertia, which could cause newly-shadowed regions not to begin trapping immediately, delay the variation enough to reproduce the data.

Unfortunately, the success of this seasonal model with the LADEE data does not continue for the long-term variation measured by LACE, which is shown by the grey points in Fig. 9 (assuming it is not the result of instrument degradation). The seasonal variation acts in the opposite way to the trend seen in 1973. Therefore, if there are seasonal cold traps that explain the LADEE argon data and they were active during the LACE measurements, then the loss rate required to match the drop measured by LACE needs to be significantly larger than had been anticipated by Grava et al. (2015). It is also noteworthy that the later LACE measurements fall well below the minimum measured by LADEE at the same location. This suggests that, if the LADEE data do show a periodic feature and there was not a transient loss event to drive down the later LACE measurements, then the equilibrium size of the exosphere must have increased over the last 40 years.

It is also possible that the LADEE and LACE long-term variations are both the result of transient source events, as suggested by Benna et al. (2015) and Grava et al. (2015). If we assume that the minima of the LADEE and LACE measurements indicate the equilibrium states throughout the measurement periods, and that a transient source had increased the density to the maximum before discontinuing, then we can model the decrease as a simple exponential decay back to the equilibrium state. In both the LADEE and LACE cases this would require a lifetime of around 0.9 lunar days, even shorter than that required for our local source bulge hypothesis and implying even greater loss rates. If the equilibrium level is lower than the minimum measurements suggest, then the variations would therefore be part of even larger but less rapid declines. In the absolute limit of no background exosphere at all, the required lifetimes could extend up to 9 and 5 lunar days for LADEE and LACE respectively. Similar arguments can be made regarding transient loss events, since LADEE shows an equally-rapid increase of argon. Of course, it is imaginable that a combination of multiple, dramatic source and loss events could produce these variations regardless of the lifetime, but this is extraordinarily unlikely.

5. Conclusions

We have studied the LADEE measurements of the lunar argon exosphere and developed a Monte Carlo model to investigate what is implied about the sources, sinks and surface interactions in the system. The extrapolation of simulated density at an altitude of 60 km to density at the surface is fitted to within 12 % everywhere using a model of two Chamberlain distributions with different temperatures. From this altitude, using a single Chamberlain distribution or its first order approximation can lead to overestimates greater than a factor of 3. These errors can be much larger for extrapolations from higher altitudes. This model fits the LADEE data well, suggesting that simple thermal desorption dominates the release energetics of exospheric argon.

The distribution with local time of day of the argon density in the exosphere is very sensitive to the nature of the interactions with the surface. Apart from an offset in amplitude reflecting the higher density over the maria, the highland and mare results are very similar, suggesting that the surface interactions do not differ greatly with regolith composition at equatorial latitudes. A model allowing atoms to squirrel into the regolith overnight, building up a subsurface population that is released during the following day, can reproduce the broad characteristics of the observed exosphere without the need to resort to unreasonably high and temperature-dependent desorption energies. The timing of the sunrise peak requires a residence time near sunrise of 1300 s, which corresponds to a desorption energy of 28 kJ mol^{-1}, a high but plausible value for noble gas interactions.

Of the two hypotheses that have been proposed for the origin of the argon bulge over the western maria, only the local source has the potential to explain this feature, with the added motivation of the near-surface overabundance of potassium. Our simulations with this model can reproduce the observed size, shape, and position of the bulge at all local times of day. However, this requires a mean lifetime for argon atoms in the exospheric system of only 1.4 lunar days, corresponding to a high equilibrium source (and loss) rate of 1.1×10^{22} atoms s^{-1}. To achieve this, our model needs permanent cold traps that have a total area comparable with the PSRs measured at Diviner's resolution, or a more highly localised source. Models that try to create the argon bulge by encouraging atoms to hop either more frequently or higher founder because they naturally lead to a short-lived feature through the night that is replaced by a local deficit in the argon density after sunrise.

The long-term variation in the global argon density seen by LADEE can be elegantly explained by the periodic behaviour of seasonal cold traps. The details of how large they need to be depend upon the size of the permanent cold traps. For the large traps that we find necessary to reproduce the bulge, extremely large seasonal traps are required that cover an additional 16 % of the polar regions at their peak. The time lag of the peak density in the data is reproduced naturally by the model for small cold traps and low rates. It is slightly offset in the high rate case, which might be explained by effects such as thermal inertia. However, the long-term decrease seen by LACE in 1973, if real, requires something more because the seasonal variation should act in the opposite way to the observed trend. The relatively smooth variation of the argon density observed over the lifetime of LADEE suggests that significant transient release or loss events are unlikely to be the cause. Any transient source (or loss) explanation would also require high rates of source and loss for the system to return to equilibrium after the event within the measured lunar-day timescales.

Seasonal cold traps should be expected to impact other species in the exosphere in a similar way, depending on their threshold trapping temperature. If any non-radiogenic, condensible species (such as methane) (Hodges, 2016) were also found to follow the variation seen for argon, then this would be strong evidence in support of the seasonal hypothesis (and vice versa), as tidal or seismic changes that might affect the argon source rate would be irrelevant for species that do not come from inside the Moon.

Experiments that could shed light on the extremely high source and loss rates that appear to be the only explanation for the bulge might be: in-situ searches for argon trapped in PSRs, although there are many uncertainties regarding how much sequestered argon would be found and at what depth (Schorghofer and Taylor, 2007); measurements of the exosphere towards the poles, where the effects that large cold traps would have on the distribution of argon with latitude would be visible; or, measurements of the late-night exosphere in the mare and highland regions. If the argon source rate does follow the near-surface potassium abundance, then the large differences in that rate should directly affect the late-night argon distributions in the two regions.

This might need to be measured at the surface to detect the very low densities. Future investigations of this kind would help determine if there is indeed such a rapid turnover of argon in the lunar exosphere.

Acknowledgements

This work was supported by the Science and Technology Facilities Council (STFC) grant ST/L00075X/1, and used the DiRAC Data Centric system at Durham University, operated by the Institute for Computational Cosmology on behalf of the STFC DiRAC HPC Facility (www.dirac.ac.uk). This equipment was funded by BIS National E-infrastructure capital grant ST/K00042X/1, STFC capital grants ST/H008519/1 and ST/K00087X/1, STFC DiRAC Operations grant ST/K003267/1 and Durham University. DiRAC is part of the National E-Infrastructure. J.A.K. is funded by STFC grant ST/N50404X/1. The LADEE and Diviner data were obtained from the NASA Planetary Data System. We thank Mehdi Benna for helpful comments regarding the processing of the LADEE data and instrument background.

References

Archinal, B. A., A'Hearn, M. F., Bowell, E., Conrad, A., Consolmagno, G. J., Courtin, R., Fukushima, T., Hestroffer, D., Hilton, J. L., Krasinsky, G. A., Neumann, G., Oberst, J., Seidelmann, P. K., Stooke, P., Tholen, D. J., Thomas, P. C., Williams, I. P., Feb. 2011. Report of the IAU Working Group on Cartographic Coordinates and Rotational Elements: 2009. Celestial Mechanics and Dynamical Astronomy 109, 101–135.

Arnold, J. R., Sep. 1979. Ice in the lunar polar regions. J. Geophys. Res.84, 5659–5668.

Benna, M., Mahaffy, P. R., Halekas, J. S., Elphic, R. C., Delory, G. T., May 2015. Variability of helium, neon, and argon in the lunar exosphere as observed by the LADEE NMS instrument. Geophys. Res. Lett.42, 3723–3729.

Bernatowicz, T. J., Podosek, F. A., 1991. Argon adsorption and the lunar atmosphere. In: Ryder, G., Sharpton, V. L. (Eds.), Lunar and Planetary Science Conference Proceedings. Vol. 21 of Lunar and Planetary Science Conference Proceedings. pp. 307–313.

Brinkmann, R. T., Apr. 1970. Departures from Jeans' escape rate for H and He in the Earth's atmosphere. Planet. Space Sci.18, 449–478.

Butler, B. J., Aug. 1997. The migration of volatiles on the surfaces of Mercury and the Moon. J. Geophys. Res.102, 19283–19292.

Chamberlain, J. W., Aug. 1963. Planetary coronae and atmospheric evaporation. Planet. Space Sci.11, 901–960.

Chaufray, J.-Y., Retherford, K. D., Gladstone, G. R., Hurley, D. M., Hodges, R. R., Jun. 2009. Lunar Argon Cycle Modeling. In: Lunar Reconnaissance Orbiter Science Targeting Meeting. Vol. 1483 of LPI Contributions. pp. 22–23.

Cheek, L. C., Donaldson Hanna, K. L., Pieters, C. M., Head, J. W., Whitten, J. L., Sep. 2013. The distribution and purity of anorthosite across the Orientale basin: New perspectives from Moon Mineralogy Mapper data. Journal of Geophysical Research (Planets) 118, 1805–1820.

Crider, D. H., Vondrak, R. R., Nov. 2000. The solar wind as a possible source of lunar polar hydrogen deposits. J. Geophys. Res.105, 26773–26782.

Dohnálek, Z., Scott Smith, R., Kay, B. D., 2002. Adsorption Dynamics and Desorption Kinetics of Argon and Methane on MgO(100). The Journal of Physical Chemistry B 106, 8360–8366.

Dunne, J. A., Mariwala, R., Rao, M., Sircar, S., Gorte, R. J., Myers, A. L., 1996. Calorimetric Heats of Adsorption and Adsorption Isotherms. 1. O2, N2, Ar, CO2, CH4, C2H6, and SF6 on Silicalite. Langmuir 12 (24), 5888–5895.

Elphic, R. C., Delory, G. T., Hine, B. P., Mahaffy, P. R., Horanyi, M., Colaprete, A., Benna, M., Noble, S. K., Dec. 2014. The Lunar Atmosphere and Dust Environment Explorer Mission. Space Sci. Rev.185, 3–25.

Farrell, W. M., Hurley, D. M., Esposito, V. J., Loeffler, M. J., McLain, J. L., Orlando, T. M., Hudson, R. L., Killen, R. M., Zimmerman, M. I., Nov. 2015. The Role of Crystal Defects in the Retention of Volatiles at Airless Bodies. In: Space Weathering of Airless Bodies: An Integration of Remote Sensing Data, Laboratory Experiments and Sample Analysis Workshop. Vol. 1878 of LPI Contributions. p. 2037.

Giorgini, J. D., Aug. 2015. Status of the JPL Horizons Ephemeris System. IAU General Assembly 22, 2256293.

Grava, C., Chaufray, J.-Y., Retherford, K. D., Gladstone, G. R., Greathouse, T. K., Hurley, D. M., Hodges, R. R., Bayless, A. J., Cook, J. C., Stern, S. A., Jul. 2015. Lunar exospheric argon modeling. Icarus255, 135–147.

Halekas, J. S., Poppe, A. R., Farrell, W. M., McFadden, J. P., Jun. 2016. Structure and composition of the distant lunar exosphere: Constraints from ARTEMIS observations of ion acceleration in time-varying fields. Journal of Geophysical Research (Planets) 121, 1102–1115.

Head-Gordon, M., Tully, J. C., Schlichting, H., Menzel, D., 1991. The coverage dependence of the sticking probability of Ar on Ru(001). J. Chem. Phys.95, 9266.

Hodges, R. R., Jan. 1980a. Methods for Monte Carlo simulation of the exospheres of the moon and Mercury. J. Geophys. Res.85, 164–170.

Hodges, R. R., Mar. 1982. Adsorption of Exospheric ARGON-40 in Lunar Regolith. In: Lunar and Planetary Science Conference. Vol. 13 of Lunar and Planetary Science Conference. pp. 329–330.

Hodges, R. R., Jul. 2016. Methane in the lunar exosphere: Implications for solar wind carbon escape. Geophys. Res. Lett.43, 6742–6748.

Hodges, R. R., Mahaffy, P. R., Jan. 2016. Synodic and semiannual oscillations of argon-40 in the lunar exosphere. Geophys. Res. Lett.43, 22–27.

Hodges, Jr., R. R., Sep. 1975. Formation of the lunar atmosphere. Moon 14, 139–157.

Hodges, Jr., R. R., 1980b. Lunar cold traps and their influence on argon-40. In: Bedini, S. A. (Ed.), Lunar and Planetary Science Conference Proceedings. Vol. 11 of Lunar and Planetary Science Conference Proceedings. pp. 2463–2477.

Hodges, Jr., R. R., Johnson, F. S., 1968. Lateral transport in planetary exospheres. J. Geophys. Res.73, 7307.

Hoffman, J. H., Hodges, Jr., R. R., Johnson, F. S., Evans, D. E., 1973. Lunar atmospheric composition results from Apollo 17. In: Lunar and Planetary Science Conference Proceedings. Vol. 4 of Lunar and Planetary Science Conference Proceedings. p. 2865.

Hurley, D. M., Sarantos, M., Grava, C., Williams, J.-P., Retherford,

K. D., Siegler, M., Greenhagen, B., Paige, D., Jul. 2015. An analytic function of lunar surface temperature for exospheric modeling. Icarus255, 159–163.

Jolliff, B. L., Gillis, J. J., Haskin, L. A., Korotev, R. L., Wieczorek, M. A., Feb. 2000. Major lunar crustal terranes: Surface expressions and crust-mantle origins. J. Geophys. Res.105, 4197–4216.

Killen, R. M., Sep. 2002. Source and maintenance of the argon atmospheres of Mercury and the Moon. Meteoritics and Planetary Science 37, 1223–1231.

Lawrence, D. J., Feldman, W. C., Barraclough, B. L., Binder, A. B., Elphic, R. C., Maurice, S., Thomsen, D. R., Sep. 1998. Global Elemental Maps of the Moon: The Lunar Prospector Gamma-Ray Spectrometer. Science 281, 1484.

Mahaffy, P. R., Richard Hodges, R., Benna, M., King, T., Arvey, R., Barciniak, M., Bendt, M., Carigan, D., Errigo, T., Harpold, D. N., Holmes, V., Johnson, C. S., Kellogg, J., Kimvilakani, P., Lefavor, M., Hengemihle, J., Jaeger, F., Lyness, E., Maurer, J., Nguyen, D., Nolan, T. J., Noreiga, F., Noriega, M., Patel, K., Prats, B., Quinones, O., Raaen, E., Tan, F., Weidner, E., Woronowicz, M., Gundersen, C., Battel, S., Block, B. P., Arnett, K., Miller, R., Cooper, C., Edmonson, C., Dec. 2014. The Neutral Mass Spectrometer on the Lunar Atmosphere and Dust Environment Explorer Mission. Space Sci. Rev.185, 27–61.

Matsuhashi, H., Tanaka, T., Arata, K., 2001. Measurement of Heat of Argon Adsorption for the Evaluation of Relative Acid Strength of Some Sulfated Metal Oxides and H-type Zeolites. J. Phys. Chem. B 105 (40).
URL http://pubs.acs.org/doi/pdf/10.1021/jp0118017

Mazarico, E., Neumann, G. A., Smith, D. E., Zuber, M. T., Torrence, M. H., Nov. 2011. Illumination Conditions of the Lunar Poles to 65 Degrees Latitude from Lunar Orbiter Laser Altimeter Data. LPI Contributions 1646, 51.

Paige, D. A., Hayne, P. O., Siegler, M. A., Smith, D. E., Zuber, M. T., Neumann, G. A., Mazarico, E. M., Denevi, B. W., Solomon, S. C., Mar. 2014. Dark Surface Deposits in the North Polar Region of Mercury: Evidence for Widespread Small-Scale Volatile Cold Traps. In: Lunar and Planetary Science Conference. Vol. 45 of Lunar and Planetary Science Conference. p. 2501.

Poppe, A. R., Halekas, J. S., Sarantos, M., Delory, G. T., Sep. 2013. The self-sputtered contribution to the lunar exosphere. Journal of Geophysical Research (Planets) 118, 1934–1944.

Prettyman, T. H., Hagerty, J. J., Elphic, R. C., Feldman, W. C., Lawrence, D. J., McKinney, G. W., Vaniman, D. T., Dec. 2006. Elemental composition of the lunar surface: Analysis of gamma ray spectroscopy data from Lunar Prospector. Journal of Geophysical Research (Planets) 111 (E10), E12007.

Schorghofer, N., Taylor, G. J., Feb. 2007. Subsurface migration of H_2O at lunar cold traps. Journal of Geophysical Research (Planets) 112, E02010.

Smith, G. R., Shemansky, D. E., Broadfoot, A. L., Wallace, L., Aug. 1978. Monte Carlo modeling of exospheric bodies - Mercury. J. Geophys. Res.83, 3783–3790.

Stern, S. A., 1999. The lunar atmosphere: History, status, current problems, and context. Reviews of Geophysics 37, 453–492.

Teodoro, L. F. A., Lawrence, D. J., Eke, V. R., Elphic, R. E., Feldman, W. C., Maurice, S., Siegler, M. A., Paige, D. A., Jan. 2015. The Local-time variations of Lunar Prospector epithermal-neutron data. ArXiv e-prints.

Vasavada, A. R., Bandfield, J. L., Greenhagen, B. T., Hayne, P. O., Siegler, M. A., Williams, J.-P., Paige, D. A., Apr. 2012. Lunar equatorial surface temperatures and regolith properties from the Diviner Lunar Radiometer Experiment. Journal of Geophysical Research (Planets) 117, 0.

Watson, K., Murray, B. C., Brown, H., Sep. 1961. The behavior of volatiles on the lunar surface. J. Geophys. Res.66, 3033–3045.

Wieczorek, M. A., Jolliff, B. L., Khan, A., Pritchard, M. E., Weiss, B. P., Williams, J. G., Hood, L. L., Righter, K., Neal, C. R., Shearer, C. K., McCallum, I. S., Tompkins, S., Hawke, B. R., Peterson, C., Gillis, J. J., Bussey, B., 2006. The Constitution and Structure of the Lunar Interior. Rev. Min. Geochem. 60, 221–364.

Wieler, R., Heber, V. S., Apr. 2003. Noble Gas Isotopes on the Moon. Space Sci. Rev.106, 197–210.

Zhu, M.-H., Chang, J., Xie, M., Fritz, J., Fernandes, V. A., Ip, W.-H., Ma, T., Xu, A., May 2015. The uniform K distribution of the mare deposits in the Orientale Basin: Insights from Chang'E-2 gamma-ray spectrometer. Earth and Planetary Science Letters 418, 172–180.

Zhu, M.-H., Ma, T., Chang, J., Tang, Z., Ip, W.-H., Xu, A., Nov. 2011. Lunar potassium distribution: Results from Chang'E-1 gamma ray spectrometer. Science China Physics, Mechanics, and Astronomy 54, 2083–2090.

A. Theory and Derivations

This appendix contains the derivation of the hop trajectory and time of flight equations. Also included are details of the 'simulation-fit' altitude model described in Section 2.1 and a short calculation concerning the squirrelling mechanism described in Section 3.

A.1. Notation

Figs. A.10(a) and (b) show all the relevant notation for a particle's hop. We use standard polar coordinates θ and ϕ, with colatitude $\theta = 0$ at the north pole, and standard selenographic longitude $\phi = 0$ at the midpoint of the Moon as viewed from Earth. The local time of day, ϕ', is given by the longitude relative to the sub-solar point (noon, where $\phi' = 0$). To account for libration, the longitude of the sub-solar point, ϕ_{ss}, is calculated from JPL HORIZONS ephemerides (Giorgini, 2015) (latitude variations are ignored). The time of day is then simply $\phi' = \phi - \phi_{ss}$. If we had ignored libration, then errors of over 3° would have been introduced for some local times of day.

A.2. Hop Trajectory

Starting from the initial position and velocity of a particle, we can calculate the landing position (or the position at any altitude) by first finding the parameters of the elliptical path, shown in Fig. A.10(a). The vis

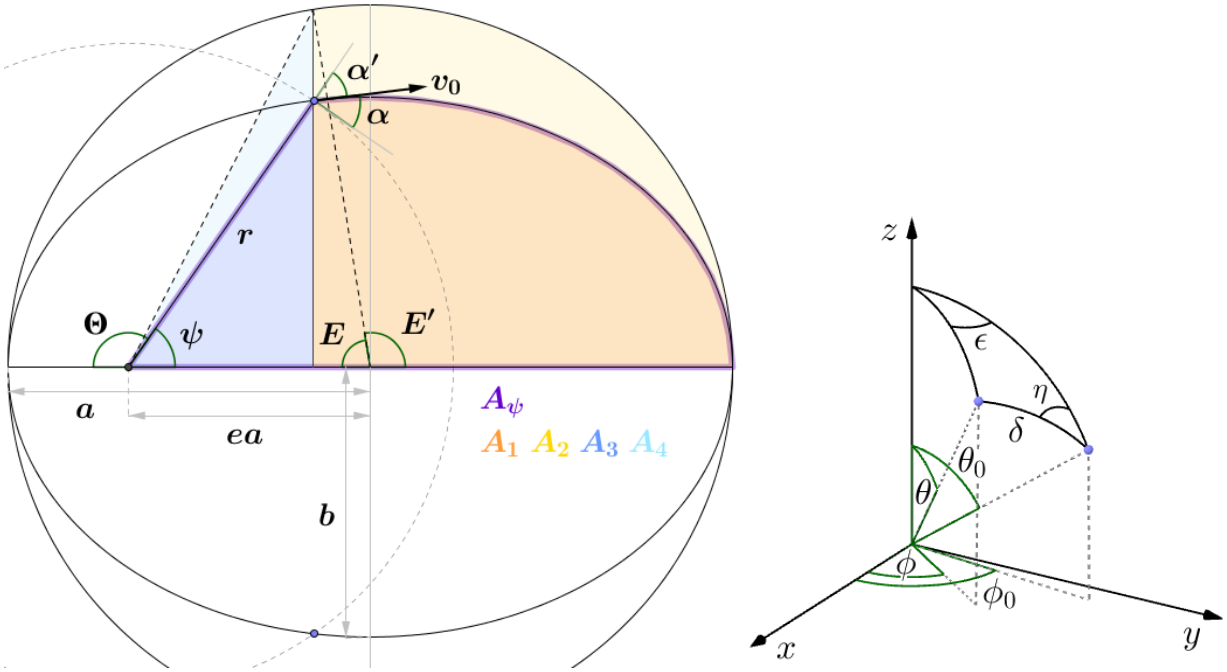

(a) Ellipse and circumcircle notation.

(b) Start and end point notation.

Figure A.10: The notation for the dimensions, angles and areas: **(a)** a, b, and e are the semi-major axis, semi-minor axis, and eccentricity of the ellipse. θ and E are the true anomaly and mean anomaly of the object at a distance r from the focus; ψ and E' are their complementary angles. α and v_0 give the velocity of the object; α' is the complementary angle. A_ψ is the area of the outlined triangle + ellipse section; A_1, A_2, A_3, and A_4 are the areas of the same-colour-shaded sections. The Moon is shown by the dashed circle; the blue points mark the start and end of a particle's hop. **(b)** The subscript 0 denotes the initial position. η is the direction west from north of the particle's initial velocity. ϵ is the difference in longitude and δ is the total angle between the start and end points.

viva equation gives the semi-major axis, a, in terms of the speed, v:

$$v^2 = GM\left(\frac{2}{r} - \frac{1}{a}\right) \quad \Rightarrow \quad a = \left(\frac{2}{r} - \frac{v^2}{GM}\right)^{-1} , \tag{A.1}$$

and the ellipticity, e, is found from the velocity angle α':

$$\sin(\alpha') = \frac{r\dot{\psi}}{v} = \sqrt{\frac{a^2(1-e^2)}{2ar - r^2}} \tag{A.2}$$

$$\Rightarrow \qquad e = \sqrt{1 - \left(\frac{2ar - r^2}{a^2}\right)\sin^2(\alpha')} \ . \tag{A.3}$$

The equation for an elliptical path can then be rearranged to give the angle ψ in terms of a and e:

$$r(\psi) = \frac{a(1-e^2)}{1 - e\,\cos(\psi)} \tag{A.4}$$

$$\Rightarrow \qquad \psi = \cos^{-1}\left[\frac{1}{e}\left(1 - \frac{a(1-e^2)}{r}\right)\right] . \tag{A.5}$$

In Fig. A.10(b), the angles δ and ϵ can be calculated along with the landing coordinates θ and ϕ. At the start of the hop ($\psi = \frac{1}{2}\delta$), Eqn. (A.5) becomes

$$\delta = 2\cos^{-1}\left[\frac{1}{e}\left(1 - \frac{a(1-e^2)}{R}\right)\right] , \tag{A.6}$$

where R is the radius of the Moon.

The spherical cosine rule gives:

$$\theta = \cos^{-1}\left[\cos(\theta_0)\cos(\delta) + \sin(\theta_0)\sin(\delta)\cos(\eta)\right] . \tag{A.7}$$

Using the cosine rule again, but with ϵ instead of η, gives

$$\epsilon = \cos^{-1}\left(\frac{\cos(\delta) - \cos(\theta)\cos(\theta_0)}{\sin(\theta)\sin(\theta_0)}\right) . \tag{A.8}$$

Then ϕ is simply given by

$$\phi = \begin{cases} \phi_0 + \epsilon & \eta > \pi \\ \phi_0 - \epsilon & \eta < \pi \end{cases} . \tag{A.9}$$

The total time of flight is $t = 2t_\psi$, where t_ψ is the time the particle spends tracing out the area A_ψ in Fig. A.10(a) with its radial vector. Using general properties of ellipses, it can be shown that $A_\psi \equiv A_1 + A_3 = \frac{b}{a}(A_2 + A_4)$, and therefore

$$A_\psi = \tfrac{1}{2}\, ab\, (E' + e\, \sin(E')) \ . \tag{A.10}$$

The total period of the orbit, T, is given by Kepler's 3rd law:

$$T = \sqrt{\frac{4\pi^2 a^3}{GM}} \ . \tag{A.11}$$

Kepler's 2nd law states that equal areas are swept out by the radial vector in equal times, therefore,

$$\begin{aligned} t_\psi &= T\frac{A_\psi}{A_{\text{ellipse}}} = T\frac{\frac{1}{2}ab(E' + e\, \sin(E'))}{\pi ab} \\ &= \frac{T}{2\pi}(E' + e\, \sin(E')) \ . \end{aligned} \tag{A.12}$$

Finally, the eccentric anomaly, E, is related to the true anomaly, Θ, by

$$E = 2\tan^{-1}\left[\sqrt{\frac{1-e}{1+e}}\tan\left(\frac{\Theta}{2}\right)\right] \ . \tag{A.13}$$

$E' = \pi - E$, $\Theta = \pi - \psi$, and here $\psi = \frac{1}{2}\delta$. Therefore,

$$E' = \pi - 2\tan^{-1}\left[\sqrt{\frac{1-e}{1+e}}\tan\left(\frac{\pi - \frac{1}{2}\delta}{2}\right)\right] \ . \tag{A.14}$$

This, with Eqn. (A.12), gives the time of flight.

A.3. Altitude Model Fitting

The 'simulation-fit' model described in Section 2.1 is a sum of two Chamberlain distributions with three free parameters: the relative amplitude of the two distributions and their different temperatures. The total amplitude is also free but is simply set by the observed density at altitude.

In order to fit these parameters at all local times of day and latitudes, we first obtained the simulated density at equilibrium for a range of altitudes (from 0 to 140 km in 10 km steps). The best-fit parameters for each square-degree bin were then determined by finding the minimum χ^2 for the simulation data.

These best-fit parameters are publicly available at icc.dur.ac.uk/index.php?content=Research/Topics/O13.

In our steady-state model, the argon density near the end of the lunar night is extremely low, especially at high latitudes and altitudes. The LADEE data in these same regions were discarded, as discussed in Section 2, so this was irrelevant for our analysis of the dataset. Thus, the best-fit parameters in these lowest-density regions were not examined in detail and may suffer from the fewer observed particles and high scatter in the simulation results.

This model is dependent on the argon distribution with time of day in the simulation. We repeated the analysis with a non-physical isotropic distribution, to quantify the maximum possible error that from discrepancies between our model and the real distribution. This amounted to ~7 % near the end of the night and below 1 % elsewhere (within ±30° latitudes).

A.4. Squirrelling

We can estimate the statistical effect this downwards migration could have on the exosphere's distribution with simple, order-of-magnitude considerations. The regolith temperature just 2 cm below the surface never drops below 200 K, and by 10 cm only varies by 15 K either side of 255 K (Teodoro et al., 2015).

For particles randomly migrating in the regolith throughout the lunar night (~10^6 s), with typical steps of size $\lambda \sim 1$ μm and residence times of $t_{\text{res}} \sim 10^{-7}$ s (for $T = 255$ K and $Q = 28$ kJ mol^{-1}), they will take $N \sim 10^{13}$ steps, random walking a distance of $\lambda\sqrt{N} \sim 1$ m. This implies that a significant number of particles could bury themselves down into the regolith during the night, with the dense source of particles residing on the surface. By symmetry (since the temperatures below the surface are similar at all times), they will take a similar amount of time to migrate out of the regolith and re-enter the exosphere. This suggests a population of particles that squirrel into the regolith during the night and typically re-enter the exosphere during the day.